ISBN: 978-3-95450-261-5 ISSN: 2673-7000 doi: 10.18429/JACoW-NAPAC2025-THP017

CALCULATIONS OF EMITTANCE MEASUREMENTS VIA INVERSE COMPTON SCATTERING*

M. Kaemingk†, P. M. Anisimov, E. I. Simakov
Los Alamos National Laboratory, Los Alamos, NM, USA
J. B. Rosenzweig
University of California, Los Angeles, CA, USA

Abstract

Recent simulation work has indicated that next generation photoinjectors will be capable of delivering beams with emittances below 100 nm for bunch charges of a few hundred pico-Coulombs. Experimentally validating these results by measuring such emittances is challenging due to the high resolution required. Additionally, in some cases it is desirable for these characterization measurements to be non-destructive, and to have the capability of selecting subsets of the beam. One technique that has been considered is the use of inverse Compton scattering (ICS) spectra to measure the emittance. Here we present simulation results on the use of ICS to measure 50 nm – 500 nm emittances for a 250 pC bunch charge electron beam.

INTRODUCTION

High brightness electron beams have become an important tool in a wide variety of applications. Thus producing and characterizing high brightness electron beams is an important area of research in accelerator physics. High gradient cold copper C-band photoinjectors provide a promising pathway for producing high brightness electron beams [1,2]. Researching this technology and demonstrating its use in producing high brightness electron beams are some of the aims of the cathodes and radio-frequency interactions in extremes (CARIE) project at Los Alamos National Laboratory (LANL) [3–5].

In previous work we have performed multi-objective optimizations studying the brightness limits of electron beams produced by the photoinjector designed for the CARIE project [6,7]. In the work reported in Ref. [6], we obtained 2D transverse normalized RMS emittances (hereafter called simply emittances) below 150 nm for beams with 250 pC per bunch. Similar work with 100 pC bunch charge beams, we find emittances below 100 nm. Additionally, in Ref. [7] we explored the use of sacrificial charge to enhance brightness following the work in Ref. [8]. In this mechanism, the initial charge is greater than the final desired charge. During non-laminar focusing of the beam, the space charge forces apply an impulse which linearizes the phase space of a subset of the beam, resulting in a bright core surrounded by diffuse tails, as shown in Fig. 1. In this way, we obtained normalized RMS emittances well below 100 nm for a final bunch charge of 250 pC.

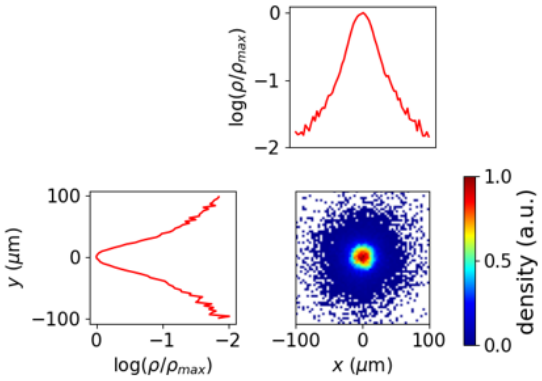

Figure 1: Example beam profile from optimizations using sacrificial charge. The top figure and bottom left figure show the log of the normalized beam profiles. There it is clear the tails do not follow a Gaussian-like distribution, but rather the existence of a halo surrounding the beam core.

Validating these simulation results requires a way to measure emittances on the 100 nm scale. In the case of the simulations with sacrificial charge, it is necessary to measure the emittance of a subset of the beam with dimensions on the scale of 10 m. The resolution required and the need for discriminating between the beam core and the surrounding tails poses a challenge for commonly used emittance measurement techniques. In this work we perform calculations exploring inverse Compton scattering (ICS) as a possible emittance measurement technique.

CALCULATION DESCRIPTION

We compute the ICS spectra in the following way. Using the Distgen package [9], we generate a particle group with properties similar to the beam properties we observed in the optimizations previously mentioned. We vary the emittance of this particle group by setting its transverse momentum spread to $mc\epsilon_n/\sigma_\perp$, where m is the electron mass, c is the speed of light, ϵ_n is the emittance, and $\sigma_\perp$ is the transverse RMS size. For each particle we then carry out the following steps:

- Generate a list of vector corresponding to incident and scattering photon directions.
- Transform the incident and scattered vectors to the particle reference frame.

* Work supported by the Laboratory Directed Research and Development program of Los Alamos National Laboratory under project number 20230011DR.
† kaemingk@lanl.gov

ISBN: 978-3-95450-261-5 ISSN: 2673-7000 doi: 10.18429/JACoW-NAPAC2025-THP017

- Compute the relativistic Doppler shift to obtain the incident wavelength in the particle rest frame.
- Calculate the scattered wavelengths in the particle rest frame from Eq. (1):

$$\lambda_{scat} = \lambda_{in} + \frac{h}{mc}(1 - \cos(\theta)), \tag{1}$$

- Calculate the scattering cross section from equation Eq. (2), the Klein-Nishina [10], which can be written as

$$\frac{d\sigma}{d\Omega} = \frac{1}{2} r_0^2 \left(\frac{\lambda_{in}}{\lambda_{scat}}\right)^2 \left(\frac{\lambda_{in}}{\lambda_{scat}} + \frac{\lambda_{scat}}{\lambda_{in}} - \sin^2(\theta)\right), \tag{2}$$

  where r_0 is the classical electron radius.
- Compute the scattered wavelengths in the laboratory reference frame.
- Compute the scattering probabilities as $P_{scat} = d\sigma \times \rho_L$, where ρ_L is the phase space density of the incident light.

The incident light distribution ρ_L is modeled as longitudinally uniform and transversely Gaussian with RMS width σ_x equal to that of the particle group. The angular distribution of the incident light is also taken to be Gaussian with RMS angular spread given by the diffraction limit $\lambda_{in}/4\pi\sigma_x$. Once this is done for all particles in the particle group, the scattered wavelengths are histogrammed, weighted by P_{scat}.

RESULTS

We performed calculations for beams with normalized RMS emittances of 50 nm, 100 nm, 200 nm and 500 nm. The incident photon wavelength is chosen to be 257 nm. This wavelength can be easily obtained by two second-harmonic generation steps from the 1030 nm laser obtained for the CARIE project. Longer wavelengths give a greater angular spread for a given laser beam size, which reduces the emittance measurement resolution.

As a proof of concept we first performed calculations with an idealized beam that has no longitudinal momentum spread. These results are shown in Figs. 2 and 3. We see no dependence of the angular distribution of the scattered photons on the emittance of the electron beam, but we observe a clear dependence on the emittance in the wavelength spectrum of the photons scattered along the electron beam direction of motion. We then performed calculations with a particle group with a more realistic longitudinal momentum spread obtained from particle tracking simulations. The energy spread greatly diminishes the emittance dependence of the ICS spectrum along the beam direction of motion. For other incident and scattering directions, however, we see a stronger dependence on emittance. These results are shown in Fig. 4.

One possible way to enhance the dependence of the scattered photon spectra on the beam emittance is by focusing the electron beam tightly. This increases the angular spread of the electron beam. Given that the wavelength of the scattered photons depends on the angle between the incident electrons

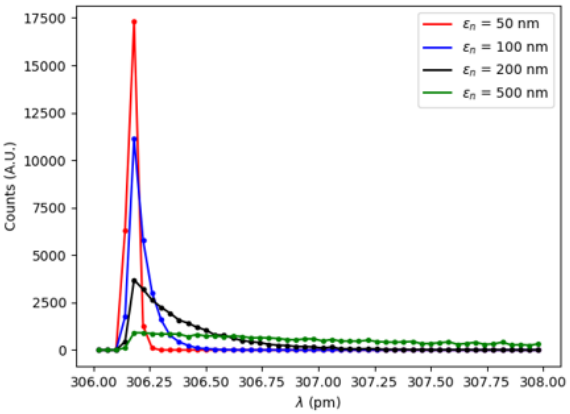

Figure 2: Spectra of photons scattered along electron beam direction of motion. Laser is incident along the direction opposite to the electron beam direction of motion. The electron beam has no longitudinal momentum spread.

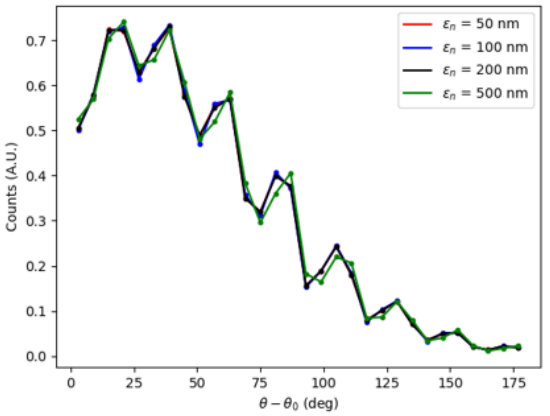

Figure 3: Angular distribution of scattered photons. Laser is incident along the direction opposite to the electron beam direction of motion. The electron beam has no longitudinal momentum spread.

and photons, this increase in the angular spread of the electrons results in a broadening of the scattered spectrum. To compute this effect, we applied a focusing transformation followed by a drift to a waist to the coordinates of the particles in the particle group, resulting in a focused particle group. With this new particle group, we performed the calculation as previously described. The results of this are shown in Fig. 5.

As expected, the wavelength spectra have been broadened. Beams with smaller emittance can be focused down to much smaller beam sizes, which implies smaller laser beam sizes as well. Since the angular spread of the laser beam is inversely proportional to its transverse size, this results in a greater angular spread in the laser beam at smaller emittances. In some configurations, this leads to the counter-intuitive result that the scattered photon spectrum is broader

ISBN: 978-3-95450-261-5 ISSN: 2673-7000 doi: 10.18429/JACoW-NAPAC2025-THP017

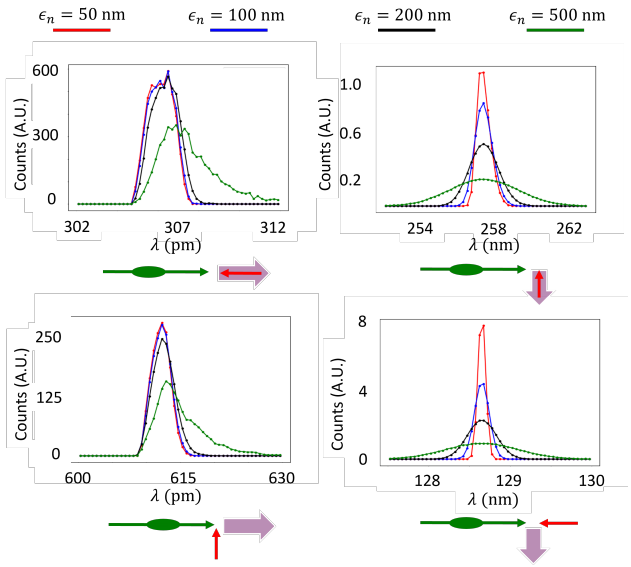

Figure 4: Spectra of scattered photons. The electron beam has an energy spread determined from particle tracking simulations with parameters obtained from optimizations. The sketches below each plot show the configuration used in the simulations. The green arrow indicated the direction of motion of the electron beam. The red arrow shows the direction of incidence of the laser. The wide, purple arrow shows the scattering direction.

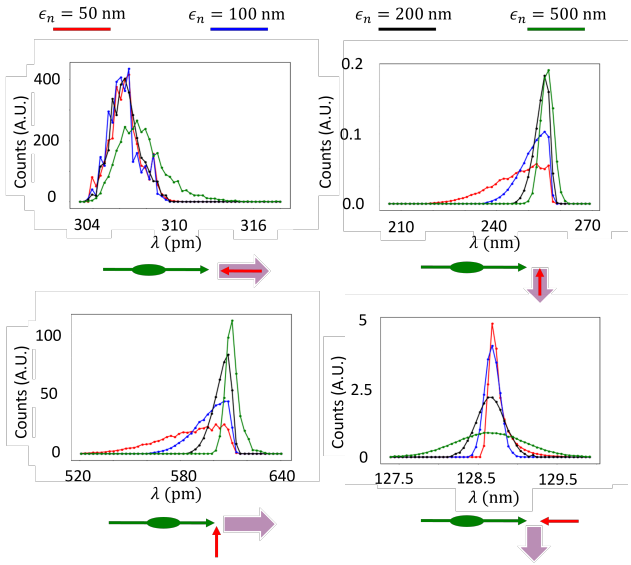

Figure 5: Spectra of scattered photons. The electron beam has been focused down to a waist, increasing its angular spread. The sketches below each plot show the configuration used in the simulations. The green arrow indicated the direction of motion of the electron beam. The red arrow shows the direction of incidence of the laser. The wide, purple arrow shows the scattering direction.

for smaller emittances, as seen in the plots at the top right and bottom left in Fig. 5.

CONCLUSION

We have performed calculations to study the use of inverse Compton scattering as means for measuring beam emittances. We find that the resolvability of the dependence of the scattered photon spectra on the electron beam emittance varies with incident and scattered photon directions, as well as with the longitudinal momentum spread of the electron beam. The dependence of the scattered photon spectrum on the emittance significantly diminishes for emittances below 100 nm. Focusing the electron beam enhances this dependence.

REFERENCES

[1] J. Rosenzweig *et al.*, "Ultra-high brightness electron beams from very-high field cryogenic radiofrequency photocathode sources", *Nucl. Instrum. Methods Phys. Res., Sect. A*, vol. 909, pp. 224–228, 2018. doi:10.1016/j.nima.2018.01.061

[2] R. R. Robles, O. Camacho, A. Fukasawa, N. Majernik, and J. B. Rosenzweig, "Versatile, high brightness, cryogenic photoinjector electron source", *Phys. Rev. Accel. Beams*, vol. 24, no. 6, p. 063 401, 2021. doi:10.1103/PhysRevAccelBeams.24.063401

[3] E. Simakov *et al.*, "Status of the CARIE high gradient photocathode test facility at LANL", in *Proc. IPAC'24*, Nashville, TN, USA, May 2024, pp. 2101–2104. doi:10.18429/JACoW-IPAC2024-WEPC60

[4] H. Xu, P. M. Anisimov, W. Barkley, and E. Simakov, "C-band photoinjector radiofrequency cavity design for enhanced beam generation", in *Proc. IPAC'23*, Venice, Italy, May 2023, pp. 2061–2063. doi:10.18429/JACoW-IPAC2023-TUPL139

[5] H. Xu *et al.*, "RF and multipactor analysis for the CARIE RF photoinjector with a photocathode insert", in *Proc. IPAC'24*, Nashville, TN, USA, May 2024, pp. 3251–3253. doi:10.18429/JACoW-IPAC2024-THPG04

[6] P. M. Anisimov, E. Simakov, H. Xu, J. Rosenzweig, J. Maxson, and M. Kaemingk, "Multi-objective genetic optimization of high charge TopGun photoinjector", in *Proc. IPAC'24*, Nashville, TN, USA, May 2024, pp. 840–843. doi:10.18429/JACoW-IPAC2024-MOPS55

[7] M. Kaemingk *et al.*, "High gradient C-band photoinjector performance utilizing sacrificial charge to enhance brightness", in *Proc. IPAC'24*, Nashville, TN, USA, May 2024, pp. 828–831. doi:10.18429/JACoW-IPAC2024-MOPS49

[8] W. H. Li *et al.*, "Compensating slice emittance growth in high brightness photoinjectors using sacrificial charge", *Phys. Rev. Accel. Beams*, vol. 27, no. 8, p. 084 401, 2024. doi:10.1103/PhysRevAccelBeams.27.084401

[9] C. Gulliford, *Distgen: Particle distribution generator, 2019*, https://github.com/ColwynGulliford/distgen.

[10] Y. Yazaki, "How the Klein–Nishina formula was derived: Based on the Sangokan Nishina source materials", *Proc. Jpn. Acad. Ser. B, Phys. Biol. Sci.*, vol. 93, no. 6, pp. 399–421, 2017. doi:10.2183/pjab.93.025